Passivity-Based Design of Plug-and-Play Current-Controlled Grid-Connected Inverters

Ali Akhavan, Hamid Reza Mohammadi, *Member, IEEE*, Juan C. Vasquez, *Senior Member, IEEE*, and Josep M. Guerrero, *Fellow, IEEE*

***Abstract*—Stable operation of *LCL* filtered grid-connected inverters can be achieved using active damping. However, the stability can be threatened by non-ideal conditions such as delay in digitally controlled systems and grid impedance variation at the point of common coupling (PCC). In a grid-side current controlled inverter, the computational and pulsewidth modulation delays cause an unintentionally negative virtual resistance when the resonance frequency is higher than one-sixth of the sampling frequency ($f_s/6$). This paper proposes a delay compensation method to address this issue, which can expand the effective damping region up to Nyquist frequency ($f_s/2$). Also, it is shown that the negative real part of the inverter output admittance will make the system unstable under specific grid condition. Therefore, a PCC voltage feedforward method is proposed to cancel the negative real part of the inverter output admittance according to passivity-based stability. Thanks to the proposed methods, the inverter output admittance will be passive in all frequencies and can be connected to the grid regardless of grid impedance. It means that the inverter has robust plug-and-play functionality. The validity of the theoretical analysis and the effectiveness of the proposed approaches are verified using experimental results on a laboratory prototype.**

***Index Terms*—Delay compensation, inverter output admittance, passivity, PCC voltage feedforward, stability.**

I. Introduction

GRID-CONNECTED inverters are the key elements for transporting renewable energy to the grid. Therefore, the quality of grid injected current is getting special attention [1], [2]. The *LCL* filter is commonly used at the output of grid-connected inverters due to its better harmonic attenuation compared with other filters such as *L* and *LC* [3]. However, the inherent resonance of the *LCL* filter is the main drawback of this kind of filter, which can cause instability of the system. For resonance damping of an *LCL* filter, passive or active damping methods could be used [4]. Passive damping methods are simple, effective, reliable, and robust. However, power loss in such kinds of damping methods is the biggest issue [5]. Hence, using active damping is getting more attention in the literature [6]–[13]. Despite higher efficiency in comparison with passive damping methods, active damping methods suffer from the delay in digitally controlled systems [14]–[16].

Delay causes major challenges such as negative virtual resistance, sampling issue, and signal aliasing. Especially, delay attracts more attention in *LCL*-filtered grid-connected inverters. Since in such systems, resonance frequency changes widely by grid impedance variation, the system stability can be threatened. The computational and pulsewidth modulation (PWM) delays in digitally controlled systems cause different behavior of active damping. Given the time delay of $1.5T_s$, where T_s is the sampling period, the grid-side current controlled systems that employed a proportional feedback of the capacitor current for active damping, will have open-loop right-half-plane (RHP) poles when the resonance frequency is higher than one-sixth of the sampling frequency ($f_s/6$), where, this frequency is named as critical frequency. RHP poles, in turn, introduce a non-minimum phase behavior to the system [17]–[20]. Therefore, increasing the sampling frequency can improve system stability. However, it is not feasible always due to hardware limitation. In this condition, using delay compensation methods can improve system stability.

Continuous research efforts have been made to amend the delay effect in the control system. To reduce the computational delay, a method is shifting the sampling instant of the capacitor current [21]. However, its implementation is susceptible to signal aliasing and switching noise. In [22], the reciprocal of a notch filter is used for compensation of the phase lag caused by the delay. However, it only expands the critical frequency up to about $f_s/4$. It is not sufficient if the resonance frequency is higher than $f_s/4$. In [23], a repetitive block is used for delay compensation, which expands the stable region up to $f_s/4$ at the cost of infinite gain and, therefore, noise amplification at the Nyquist frequency ($f_s/2$), which practically may not be permitted. In [7], a first-order high-pass filter is used in the active damping loop for delay compensation. This method is simple, but the improvement is limited to $f_s/3$ and it is not effective when the resonance frequency is higher than $f_s/3$. On the other hand, to achieve the delay compensation up to $f_s/3$, the cut-off frequency of high-pass filter should be selected as $3\omega_s$ (ω_s is sampling frequency in rad/s), which is not applicable because of possible noise amplification. Therefore, the compensation area is below $f_s/3$ in practice. In [24], Qian *et al.* proposed a proportional quasi-resonant controller, which expands the critical

Manuscript received January 26, 2019; revised April 12, 2019; accepted May 30, 2019. Date of publication June 4, 2019; date of current version November 12, 2019. Recommended for publication by Associate Editor Y. Xue. *(Corresponding author: Hamid Reza Mohammadi.)*

A. Akhavan and H. R. Mohammadi are with the Department of Electrical and Computer Engineering, University of Kashan, Kashan, Iran (e-mail: aliakhavan@grad.kashanu.ac.ir; mohammadi@kashanu.ac.ir).

J. C. Vasquez and J. M. Guerrero are with the Department of Energy Technology, Aalborg University, Aalborg 9220, Denmark (e-mail: juq@et.aau.dk; joz@et.aau.dk).

Color versions of one or more of the figures in this paper are available online at http://ieeexplore.ieee.org.

Digital Object Identifier 10.1109/TPEL.2019.2920843

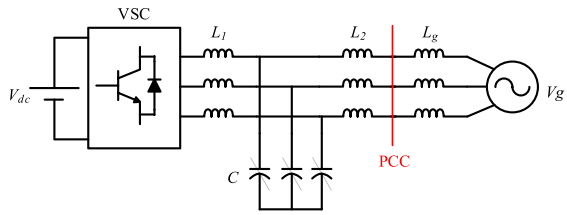

Fig. 1. Typical three phase grid-connected inverter with the *LCL* filter.

frequency up to $0.358 f_s$. However, the limitation of the proposed method is similar to [7] and [23]. Another method used in [25] is the capacitor current prediction with an observer. However, this method is sensitive to parameter variations and uncertainties. Hence, it may lose its optimal performance in case of parameters mismatch. In [26], a double-sampling-based method is proposed for delay compensation, which complicates the control system with additional computation. In this paper, a new method is proposed, which can expand the effective damping region up to Nyquist frequency $(f_s/2)$ using a biquad filter. The proposed method does not have the mentioned limitations.

Another factor that normally challenges the stability of the grid-connected inverters is the grid impedance. It can be regarded as a part of the grid-side inductor of the *LCL* filter as shown in Fig. 1. In this way, it directly affects the bandwidth, phase margin (PM), and gain margin (GM) of the control system [27]. The main difficulty is the grid impedance variation that may vary widely in weak grids. Additionally, for a system containing multiple paralleled inverters connected to the point of common coupling (PCC), the equivalent grid impedance, which is seen by each inverter becomes larger than the actual grid impedance, probably resulting instability [28]–[30]. Inverter output admittance can be used for stability assessment according to impedance-based stability criterion in grid-connected systems [31]. Despite using active damping, the real part of inverter output admittance would be negative in the vicinity of resonance frequency [32]. Although small, if the grid admittance intersects with inverter output admittance in such frequency range, it impairs the overall system stability and robustness. This situation is very probable in weak grids with a wide variation of the grid impedance. Adaptive algorithms based on online grid impedance estimation are proposed to solve this problem, which tunes the control parameters according to grid impedance [27], [33]. However, these methods will burden the control system with additional computation.

The passivity concept, which has been increasingly studied, provides an attractive way to analyze the harmonic stability problem and design recommendations for minimizing the frequency range in which the real part of inverter output admittance is negative [34]. Passivity-based stability provides design guideline for all connected sub-systems to have passive behavior. The passivity of the inverter output admittance is guaranteed using this method, and therefore, the inverter connection will not destabilize the system. In this condition, the system is stable regardless of the grid impedance and the number of parallel inverters, since each component is solely passive in all frequencies. In [30], it is shown how the non-passive grid-connected inverters interact with the varying grid impedance. Bai *et al.* [35] proposed a series *LC*-filtered active damper to mimic a damping resistance at the resonance frequencies and the passivity concept is used for selection of damping resistance. However, adding an extra converter for resonance damping complicates the control system and increases the cost.

The similar idea is proposed in [36], which an active filter is used for cancelation of grid impedance. In [37], the inverter output admittance is decomposed into a passive admittance in series with an active admittance, which the former is dependent on the *LCL* filter and the latter is dependent on the current controller and the time delay. A capacitor voltage feedforward method is proposed in [38] for active damping and passivity of inverter output admittance. However, the effect of the capacitor voltage loop on inverter stability is not discussed. In [39], the *LCL* filter parameters are designed so that inverter can work in the passive region. However, the *LCL* filter parameters should be designed to attenuate the switching harmonic components effectively and selecting these parameters based on passivity can reduce the performance of the *LCL* filter in its main task. Harnefors *et al.* [40] used a modified resonance controller to amend the phase of inverter output admittance. However, a passive inverter can only guarantee the system stability, but it cannot guarantee the required PM.

In this paper, the passivity is achieved using the PCC voltage feedforward method. It guarantees the stability of the grid-connected inverter by a sufficient PM regardless of grid impedance value and the number of parallel inverters. Thanks to the proposed methods, the real part of inverter output admittance remains positive in all frequencies and inverter has plug-and-play functionality. The contributions of this paper can be summarized as follows.

1) A novel delay compensation method is proposed, which expands the critical frequency up to Nyquist frequency.
2) The passivity-based stability of the grid-connected inverters is enhanced using a new PCC voltage feedforward method and its plug-and-play operation is guaranteed.

The rest of this paper is organized as follows. In Section II, an overall description of the delay effect is briefly presented to formulate the problem. The delay compensation method is proposed in Section III to expand the critical frequency. The passivity-based stability is considered in Section IV and a PCC voltage feedforward loop is designed to achieve the plug-and-play functionality. In Section V, the proposed methods are validated through experimental results on a lab prototype. Finally, Section VI concludes the paper.

II. System Description and Problem Definition

A three-phase grid-connected voltage source inverter with an *LCL* filter is shown in Fig. 1. In this figure, L_1, $L_{2,}$, and C are the inverter-side inductor, the grid-side inductor, and the filter capacitor, respectively. Also, L_g represents the grid inductance that contains line inductance and transformer leakage inductance. The grid inductance may vary over a wide range. Hence, the control system should be designed robustly so that it does not degrade significantly as L_g varies. The resistive components tend to make the system more stable.

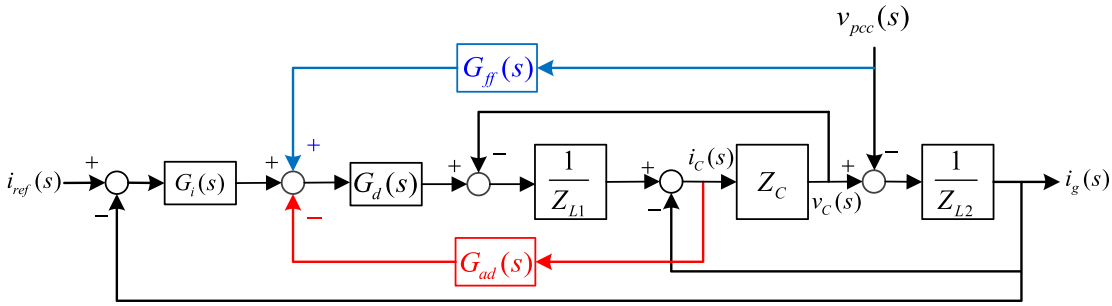

Fig. 2. Block diagram of the dual-loop control strategy based on capacitor current feedback active damping and PCC voltage feedforward.

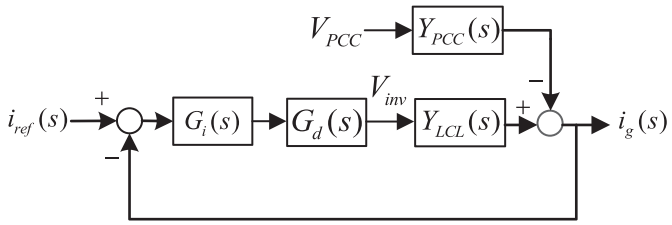

Fig. 3. Simplified block diagram of Fig. 2 without active damping and PCC voltage feedforward.

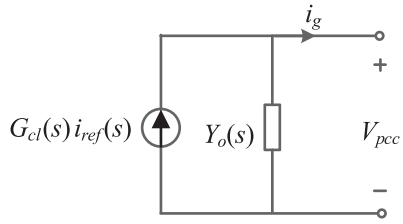

Fig. 4. Norton equivalent circuit of the grid-connected inverter.

Therefore, the reactive components are only considered to study the worst-case condition. The dc-link voltage is regarded as constant for simplicity and bandwidth of the phase-locked loop (PLL) is designed smaller than the grid fundamental frequency to avoid unintentional low-frequency interaction. In this paper, the bandwidth of the PLL is selected as 25 Hz. Hence, the PLL loop can be neglected [41], [42].

Per-phase control block diagram of the grid-connected inverter with *LCL* filter, which uses dual-loop active damping scheme with capacitor current feedback is presented in Fig. 2. In this figure, $G_i(s)$ is the current controller and Z_{L1}, Z_{L2}, Z_C, and Z_g are the impedances related to L_1, L_2, C, and L_g, respectively. The PR controller in (1) is used as current controller, where, $\omega_0 = 2\pi f_0$ and f_0 is the fundamental frequency. $G_{ad}(s)$ is the active damping controller, and i_C is the capacitor current, which is fed back and passes through $G_{ad}(s)$ to damp the *LCL* filter resonance. Also, $G_{ff}\,(s)$ is the controller for PCC voltage feedforward. In addition, $G_d(s)$ models the computational and the PWM delay [7]

$$G_i(s) = k_p + \frac{k_r s}{s^2 + \omega_0^2} \tag{1}$$

$$G_d(s) = e^{-1.5\,T_s s}. \tag{2}$$

A. Non-Passive Region Without Active Damping and PCC Voltage Feedforward

To show the necessity of the active damping method for system stability, the non-passive region of inverter output admittance without using any damping method is extracted here. Supposing that $G_{ad}(s) = 0$ and $G_{ff}(s) = 0$, the block diagram of the dual-loop control system of Fig. 2 can be simplified to a single-loop system, as shown in Fig. 3. In this figure, $Y_{LCL}(s)$ is the transfer function between inverter output voltage ($V_{\rm inv}$) and grid-injected current and $Y_{\rm PCC}(s)$ is the transfer function between PCC voltage and grid-injected current. These transfer functions are given in the following equations:

$$Y_{LCL}(s) = \left.\frac{I_g(s)}{V_{\rm inv}(s)}\right|_{V_{\rm PCC}=0} = \frac{Z_C}{Z_{L1}Z_{L2} + Z_{L1}Z_C + Z_{L2}Z_C}$$
$$= \frac{1}{s^3 L_1 L_2 C + s(L_1 + L_2)} \tag{3}$$

$$Y_{\rm PCC}(s) = \left.\frac{I_g(s)}{-V_{\rm PCC}(s)}\right|_{V_{\rm inv}=0} = \frac{Z_{L1} + Z_C}{Z_{L1}Z_{L2} + Z_{L1}Z_C + Z_{L2}Z_C}$$
$$= \frac{s^2 L_1 C + 1}{s^3 L_1 L_2 C + s(L_1 + L_2)}. \tag{4}$$

According to Fig. 3 and (3) and (4), the inverter output admittance can be calculated as follows:

$$Y_O(s) = \left.\frac{I_g(s)}{-V_{\rm PCC}(s)}\right|_{I_{\rm ref}=0} = \frac{Y_{\rm PCC}}{1 + G_i(s)G_d(s)Y_{LCL}(s)}$$
$$= \frac{s^2 L_1 C + 1}{s^3 L_1 L_2 C + s(L_1 + L_2) + G_i(s)G_d(s)}. \tag{5}$$

The Norton equivalent circuit of an inverter is shown in Fig. 4, where $G_{cl}(s)$ is the closed-loop transfer function of the control system, which can be obtained using Fig. 3 as follows:

$$G_{cl}(s) = \frac{I_g(s)}{I_{\rm ref}(s)} = \frac{G_i(s)G_d(s)Y_{LCL}(s)}{1 + G_i(s)G_d(s)Y_{LCL}(s)}. \tag{6}$$

The resonant part of PR controller can be neglected at frequencies not in the vicinity of the fundamental frequency because of its negligible effect at these frequencies [38], [43]. Hence, assuming that $G_i(s) \approx k_p$, the inverter output admittance can be simplified as follows:

$$Y_O(s) = \frac{s^2 L_1 C + 1}{s^3 L_1 L_2 C + s(L_1 + L_2) + k_p G_d(s)}. \tag{7}$$

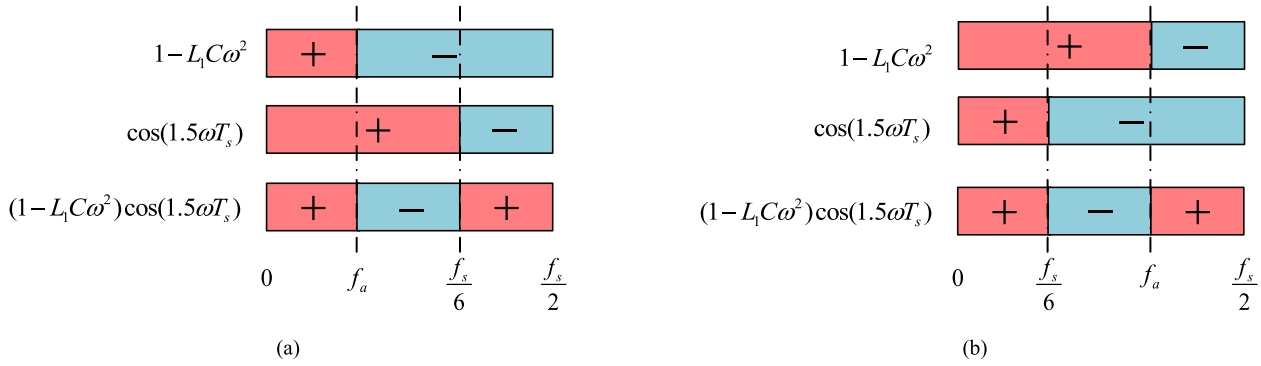

Fig. 5. Non-passive region of the output admittance of a grid-connected inverter with the *LCL* filter. (a) $f_a < f_s/6$. (b) $f_a > f_s/6$.

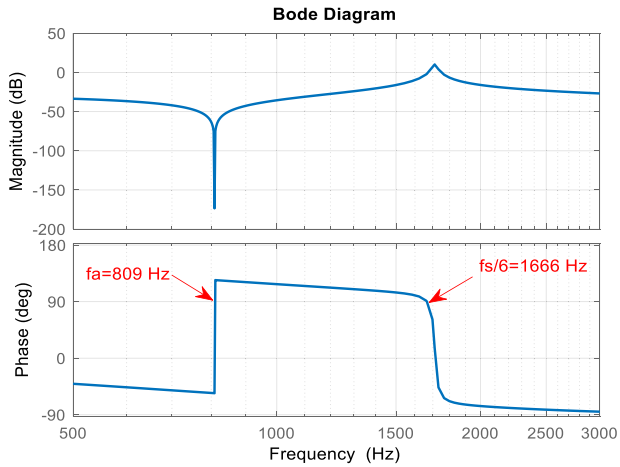

Fig. 6. Bode plot of inverter output admittance without using active damping.

TABLE I
PARAMETERS OF THE INVERTER AND GRID

Parameters of inverter	
Input DC voltage, V_{dc}	650 V
Inverter-side inductor, L_1	8.6 mH (0.0371 p.u)
Filter capacitor, C	4.5 μF (0.1028 p.u)
Grid-side inductor, L_2	1.8 mH (0.0078 p.u)
LCL resonance frequency	1945 Hz
Sampling and switching frequency	10 kHz
Rated power of each inverter	2.2 kVA
Parameters of utility grid	
Grid Voltage, V_g (Phase-to-phase RMS Voltage)	400 V
Frequency	50 Hz
Grid inductance, L_g	0 / 1.8 mH / 5.4 mH 0 / 0.0078 p.u / 0.0234 p.u

The inverter output admittance has an anti-resonance peak at f_a, which derives from complex conjugate zeros in (7) and is given by

$$f_a = \frac{1}{2\pi\sqrt{L_1 C}}. \tag{8}$$

Using (7) and mathematical simplification, the real part of $Y_O(s)$ can be achieved as eq. (9) shown at the bottom of this page.

The denominator of (9), is always positive. Hence, it does not affect the passivity of the inverter. However, positivity or negativity of the real part of $Y_O(s)$ can be investigated according to the numerator of (9). According to this, it can be easily concluded that the real part of $Y_O(s)$ is negative in the interval of $(f_a,\ f_s/6)$ when f_a is below $f_s/6$. Also, when f_a is higher than $f_s/6$, the real part of $Y_O(s)$ is negative in the interval of $(f_s/6,\ f_a)$, which is shown in Fig. 5 graphically.

The Bode plot of $Y_O(s)$ is shown in Fig. 6 using the parameters listed in Table I and assuming $k_p = 1$. Based on impedance-based stability criterion, for the stability of parallel connection of two stable sub-systems (here, inverter and utility grid), their output admittance must have a positive PM at the intersection point (f_i) [31], i.e.,

$$\mathrm{PM} = 180^\circ - [\angle Y_o(f_i) - \angle Y_g(f_i)]. \tag{10}$$

As shown in Fig. 6, there is a wide range of frequency $(f_a < f < f_s/6)$, which the phase of $Y_O(s)$ is beyond $[-90^\circ, 90^\circ]$. Noting that if the grid admittance, which is commonly inductive due to line inductance and transformer leakage inductance, intersects with inverter output admittance in such frequency range, it impairs the system stability. Therefore, to guarantee the stability of a grid-connected inverter, a damping method must be employed. Active damping methods are getting more attention due to the higher efficiency with respect to passive methods. However, delay in digitally controlled systems brings new challenge, which is briefly explained in the following section.

$$\mathrm{Re}\{Y_O(s)\} = \frac{k_p(1-L_1C\omega^2)\cos(1.5\omega T_s)}{[k_p\cos(1.5\omega T_s)]^2 + [-\omega^3 L_1 L_2 C + (L_1+L_2)\omega - k_p\sin(1.5\omega T_s)]^2} \tag{9}$$

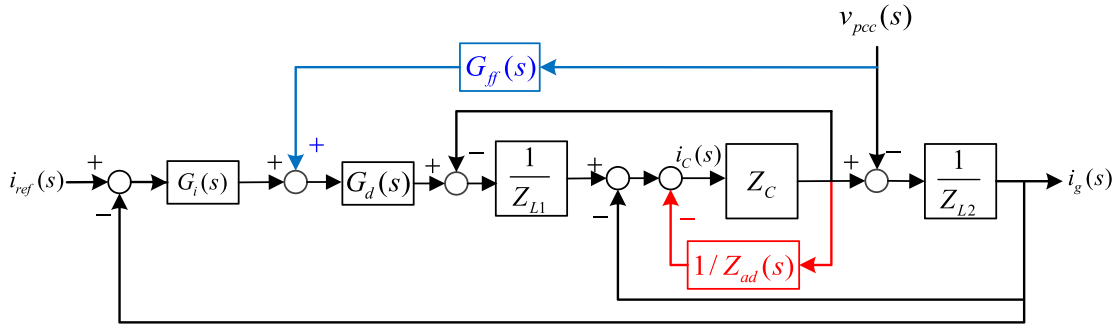

Fig. 7. Equivalent representation of capacitor current feedback based active damping.

B. Delay Effect on the Active Damping

According to the above-mentioned analysis, using a damping method based on passivity theory is necessary to mitigate the resonance and to shrink the non-passive region. Dual-loop active damping control based on capacitor current feedback such as Fig. 2 is commonly used because of its simple and effective implementation. Block diagram of Fig. 2 can be transformed into Fig. 7 using signal flow graph simplification rules. The active damping based on capacitor current feedback is equal to inserting a virtual impedance Z_{ad} in parallel with the filter capacitor [19] as follows:

$$Z_{ad}(s) = \frac{L_1}{CG_{ad}(s)G_d(s)}. \tag{11}$$

In the active damping method based on capacitor current feedback, normally a proportional controller is used ($G_{ad}(s) = K_{ad}$). Therefore, $Z_{ad}(s)$ can be represented as follows:

$$Z_{ad}(s) = \frac{L_1}{CK_{ad}}\left[\cos(1.5\omega T_s) + j\sin(1.5\omega T_s)\right]. \tag{12}$$

According to (12), the real part of virtual impedance Z_{ad} is positive in the range of $(0,\ f_s/6)$ and negative in the range of $(f_s/6,\ f_s/2)$. Therefore, it implies that the loop gain might have RHP poles if the *LCL* filter resonance frequency is located between $f_s/6$ and the Nyquist frequency $f_s/2$, which in turn, causes the instability of the control system [19]. Hereinafter, the frequency at which virtual impedance becomes negative is named as critical frequency f_{cr}. In [20], it is shown that without using active damping, the system has an inherent damping effect when the resonance frequency is higher than $f_s/6$. However, this feature is not attractive in practice because according to (13), which shows resonance frequency in weak grids [8], wide variation of grid impedance can shift the resonance frequency below $f_s/6$. Therefore, in order to guarantee the system stability despite wide variation of grid impedance, a robust active damping method should be used for compensation of the delay effect

$$f_r = \frac{1}{2\pi}\sqrt{\frac{L_1 + L_2 + L_g}{L_1(L_2 + L_g)C}}. \tag{13}$$

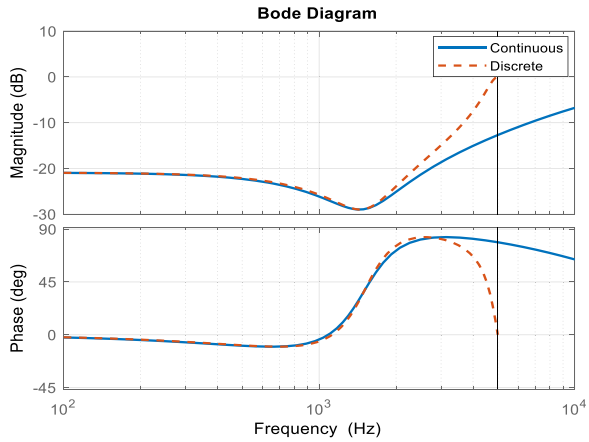

Fig. 8. Bode plot of a typical biquad filter in continuous and discrete domains.

III. Delay Compensation Based on the Biquad Filter

In this section, the biquad filter and how to tune its parameters are addressed.

A. Biquad Filter

In order to enhance the active damping method to guarantee the stability of a grid-connected inverter against the grid impedance variation, the critical frequency should be increased to prevent introducing RHP poles. To do this, the phase lag associated with time delay should be compensated. Some of delay compensation methods are explained in Section I, which have some problems. To cope with these problems, a biquad filter is proposed to compensate the phase lag and keep the virtual impedance positive over a wide range of frequency. The biquad filter is used as an active damping controller $G_{ad}(s)$, which is the best place for compensation of delay effect in the capacitor current feedback based active damping method [22]. Hence, $G_{ad}(s)$ can be expressed as (14), instead of using a proportional controller

$$G_{ad}(s) = K_{ad}\frac{s^2 + 2\alpha\,\omega_\alpha s + \omega_\alpha^2}{s^2 + 2\beta\,\omega_\beta s + \omega_\beta^2} = K_{ad}\frac{G_{ad\_\mathrm{num}}(s)}{G_{ad\_\mathrm{den}}(s)}. \tag{14}$$

The Bode plot of a typical biquad filter is plotted in Fig. 8 ($K_{ad} = 1$). As shown in this figure, the biquad filter can be

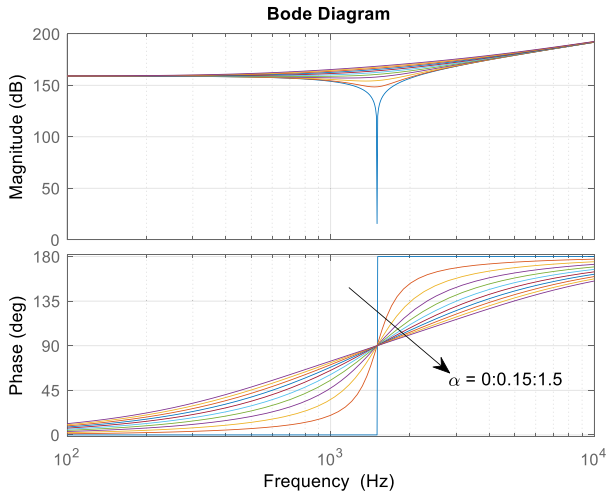

Fig. 9. Bode plot of $G_{ad\_\mathrm{num}}(s)$.

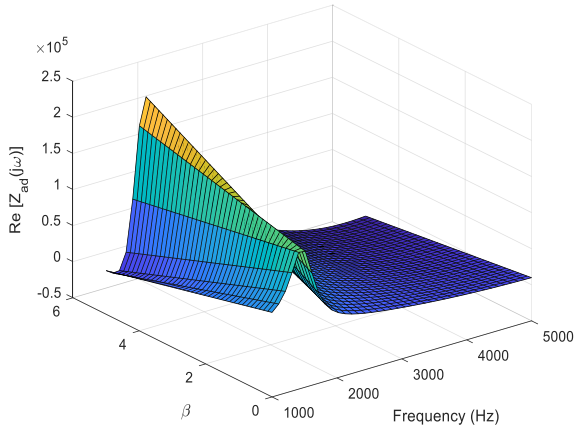

Fig. 10. Real part of virtual impedance Z_{ad} versus β and frequency.

used for compensation of the delay oriented phase lag by introducing positive phase in the desired frequency range. For digital realization of the biquad filter, the Tustin method is used in this paper while the prewarp frequency is set to 1500 Hz [44]. Pan *et al.* [45] provided an approach for digital realization of transfer function containing differentiator, which can be used for digital realization of the biquad filter, as well.

B. Tuning Biquad Filter Parameters

The gain of the biquad filter (K_{ad}) should be selected to damp the resonance peak since it only affects the magnitude of virtual impedance and has no effect on phase compensation. The other parameters, i.e., α, β, ω_α, and ω_β should be selected to introduce the desirable positive phase. The delay $G_d(s)$ introduces $-90°$ phase lag at $\omega_s/6$. On the other hand, the numerator of $G_{ad}(s)$, i.e., $G_{ad\_\mathrm{num}}(s)$ introduces $+90°$ phase lead at ω_α. Therefore, if ω_α be equal to $\omega_s/6 \approx 0.16\omega_s$, the phase lag will be compensated by $G_{ad}(s)$. Note that slight derivation has no significant effect on the effectiveness of the control system. Hence, ω_α is selected as $0.15\omega_s$ in this paper.

Fig. 9 shows the Bode plot of $G_{ad\_\mathrm{num}}(s)$ and helps for tuning α, where α is swept from 0 to 1.5 with a step size of 0.15. As shown in this figure, lower values for α introduce more phase lag compensation in higher frequencies. However, $\alpha = 0$ causes a notch filter behavior for active damping loop, which prevents measuring of all frequencies. On the other hand, phase compensation in $\omega < \omega_\alpha$ is zero when $\alpha = 0$, which is not preferable. Therefore, 0.15 is the soundest choice for α.

The denominator of $G_{ad}(s)$, i.e., $G_{ad\_\mathrm{den}}(s)$ should be designed so that keep the magnitude of $G_{ad}(s)$ in a reasonable range in high frequencies to prevent noise amplification. Also, according to the main purpose of the biquad filter which is delay compensation and introducing positive phase up to Nyquist frequency, ω_β should be selected higher than $\omega_s/2$. Therefore, ω_β is selected as $0.7\omega_s$, which is a fair tradeoff between the magnitude of $G_{ad}(s)$ in high frequencies and positive phase introducing up to Nyquist frequency.

A graphical method is used for tuning β. Note that the main purpose of using the biquad filter is to keep the real part of virtual impedance (Z_{ad}) positive as high frequency as possible. Therefore, using (11) and (14), the real part of Z_{ad} can be achieved as (15) shown at the bottom of the next page.

Using system parameters listed in Table I and $K_{ad} = 1$, $\omega_\alpha = 0.15\omega_s$, $\omega_\beta = 0.7\omega_s$, and $\alpha = 0.15$, the desired value for β can be obtained using Fig. 10. This figure shows the real part of Z_{ad} versus β and frequency. As shown in Fig. 10, by selecting β smaller than 2, the real part of the virtual impedance remains positive up to the Nyquist frequency, which is a great achievement, with respect to the situation that only a proportional gain is used. According to Fig. 10, in this paper, β is selected as 1 for phase compensation. After tuning ω_α, ω_β, α, and β, the gain of the biquad filter (K_{ad}) can be designed. Through numerous simulations, it is found that a 100 Ω virtual resistor damps the resonance. By solving (11) in resonance frequency, K_{ad} can be achieved as 400.

IV. Passivity Enhancement Using PCC Voltage Feedforward

As stated in passivity-based theory, a grid-connected inverter will be stable if its output admittance is passive in all frequencies. In other words, it should satisfy the following constraints: 1) the closed-loop transfer function of the control system should not have RHP poles and 2) the real part of the inverter output admittance should be non-negative [37]. The first constraint implies that the inverter is internally stable [28]. According to these constraints, whole of the system will be stable regardless of the grid impedance and the number of parallel grid-connected inverters at the PCC.

Active damping methods can shrink the non-passive region of the inverter output admittance. However, it would remain a narrow region in the vicinity of resonance frequency, which the phase of output impedance is beyond $[-90°, 90°]$. Although small, if the grid admittance and inverter output admittance magnitudes intersect in such frequency range, it impairs the overall system stability and robustness. It endangers the stability of the system especially in weak grids whose grid impedance varies

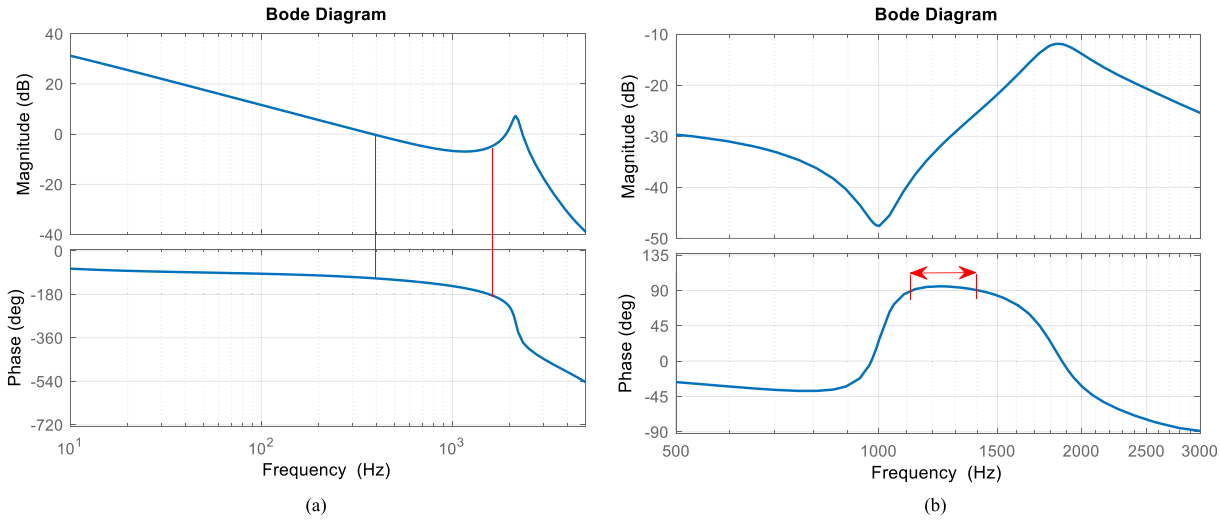

Fig. 11. (a) Bode plot of the control system loop gain. (b) Bode plot of inverter output admittance using the proposed active damping based on delay compensation and without PCC voltage feedforward method ($G_{ff}(s) = 0$).

widely. Even if the phase of inverter output admittance remains within $[-90°, 90°]$, the quality of grid-injected current will be unacceptable in case of insufficient PM. Hence, in this paper, the passivity-based stability is used, to mitigate the non-passive region and to guarantee the satisfactory operation of the grid-connected inverter by a sufficient PM.

To investigate the inverter behavior and design a control system to guarantee its passivity in all frequencies, the control system loop gain and the inverter output admittance can be derived from Fig. 2 as (16) and (17), respectively. For simplicity, in these transfer functions, the current controller is considered as a proportional controller ($G_i(s) \approx k_p$). By considering $k_p = 25$, the Bode plots of loop gain and inverter output admittance are shown in Fig. 11(a) and (b), respectively. Note that in Fig. 11(b), the PCC voltage feedforward is not used ($G_{ff}(s) = 0$), while it does not affect loop gain according to (16)

$$T(s) = \frac{k_p G_d Z_C}{Z_{L1}Z_{L2} + Z_{L1}Z_C + Z_{L2}Z_C + G_{ad}G_d Z_{L2}} = \frac{k_p G_d}{s^3 L_1 L_2 C + s(L_1 + L_2) + s^2 L_2 C G_{ad} G_d} \tag{16}$$

$$Y_O(s) = \frac{Z_{L1} + Z_C + G_{ad}G_d - G_{ff}G_d Z_C}{Z_{L1}Z_{L2} + Z_{L1}Z_C + Z_{L2}Z_C + k_p G_d Z_C + G_{ad}G_d Z_{L2}} = \frac{s^2 L_1 C + 1 + sCG_{ad}G_d - G_{ff}G_d}{s^3 L_1 L_2 C + s(L_1 + L_2) + k_p G_d(s) + s^2 L_2 C G_{ad} G_d}. \tag{17}$$

As shown in Fig. 11(a), the closed-loop control system is stable because PM>0 and also, the magnitude of loop gain is below 0 dB, where the phase curve crosses $-180°$ [19]. However, the Bode plot of loop gain is shown without considering the grid impedance. Therefore, the system might lose its stability when it connects to a weak grid. The best way for stability assessment of an inverter in weak grid condition is investigation of the inverter output admittance, which is plotted in Fig. 11(b). In comparison with Fig. 6, the non-passive region is mitigated using the proposed active damping without the PCC voltage feedforward method. However, there still exists a frequency range at which the phase is over 90°.

To remove the non-passive region, the active damping gain (K_{ad}) can be increased as shown in Fig. 12. According to this figure, with increasing K_{ad}, the non-passive region is mitigated. However, the PM might be insufficient, which results in the poor transient performance and power quality. To achieve a satisfactory PM, the PCC voltage feedforward method is proposed in this paper. To reduce the phase of $Y_O(s)$, the phase of its numerator is reduced. According to (17), the numerator of $Y_O(s)$ is given as follows:

$$\text{Num}\{Y_O(s)\} = Y_N(s) = s^2 L_1 C + 1 + sCG_{ad}G_d - G_{ff}G_d = Y_u - G_{ff}G_d \tag{18}$$

where $Y_u = s^2 L_1 C + 1 + sCG_{ad}G_d$. Due to the second-order derivative element in Y_u, its phase can be regarded approximately equal to 180° at medium and high frequencies ($\angle Y_u \approx 180°$). Therefore, according to Fig. 13, a low-pass filter, as (19), is the soundest choice for $G_{ff}(s)$ to reduce the phase

$$\text{Re}\{Z_{ad}(j\omega)\} = \frac{L_1}{CK_{ad}} \frac{1}{(\omega_\alpha^2 - \omega^2)^2 + (2\alpha\omega_\alpha\omega)^2} \times \big((\omega_\alpha^2 - \omega^2)(\omega_\beta^2 - \omega^2)\cos(1.5\omega T_s) + (2\alpha\omega_\alpha\omega)(2\beta\omega_\beta\omega)\cos(1.5\omega T_s) + (\omega_\beta^2 - \omega^2)(2\alpha\omega_\alpha\omega)\sin(1.5\omega T_s) - (\omega_\alpha^2 - \omega^2)(2\beta\omega_\beta\omega)\sin(1.5\omega T_s)\big) \tag{15}$$

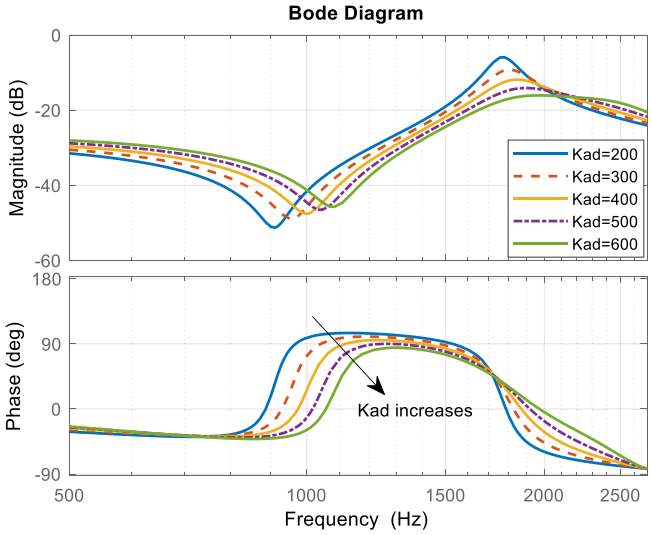

Fig. 12. Bode plot of inverter output admittance using the proposed active damping with various K_{ad} and $G_{ff}(s) = 0$.

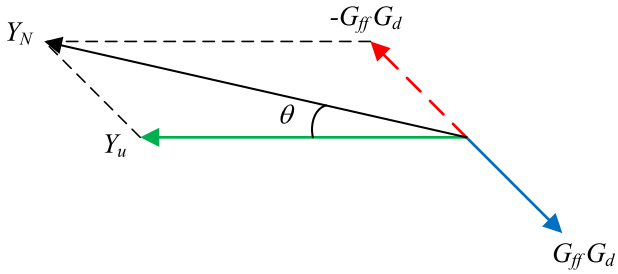

Fig. 13. Phasor diagram of numerator of $Y_O(s)$.

of the numerator of $Y_O(s)$

$$G_{ff}(s) = k_{ff}\frac{\omega_f}{s+\omega_f}. \tag{19}$$

In (19), k_{ff} and ω_f are gain and cutoff frequency of the low-pass filter, respectively. Therefore, According to Fig. 13, the phase of the numerator of $Y_O(s)$ can be reduced by $\theta°$ in the desired frequency range. Fortunately, the non-passive region of inverter output admittance is in the vicinity of the resonance frequency, i.e., in medium and high frequencies, and hence, supposing $\angle Y_u \approx 180°$ is acceptable. In the following, the low-pass filter parameters are designed to guarantee the passivity of inverter output admittance in all frequencies.

According to Fig. 12, the interesting frequency range at which the phase of $Y_O(s)$ should be decreased is less than 2000 Hz. Therefore, ω_f is selected as $2\pi\times2000$ (rad/s). Due to the low magnitude of $G_{ff}(s)$ in frequencies higher than 2000 Hz, it does not affect $Y_O(s)$. Hence, it does not cause that phase of $Y_O(s)$ exceed $-90°$ in frequencies higher than 2000 Hz. To design the coefficient of the low-pass filter (k_{ff}), a graphical method is used, which is an intuitive designing method. In Fig. 14, the phase of $Y_O(s)$ versus frequency and k_{ff} is plotted. As shown in this figure, by increasing k_{ff}, the phase of $Y_O(s)$ is decreased in medium and high frequencies (frequencies higher than 1000 Hz),

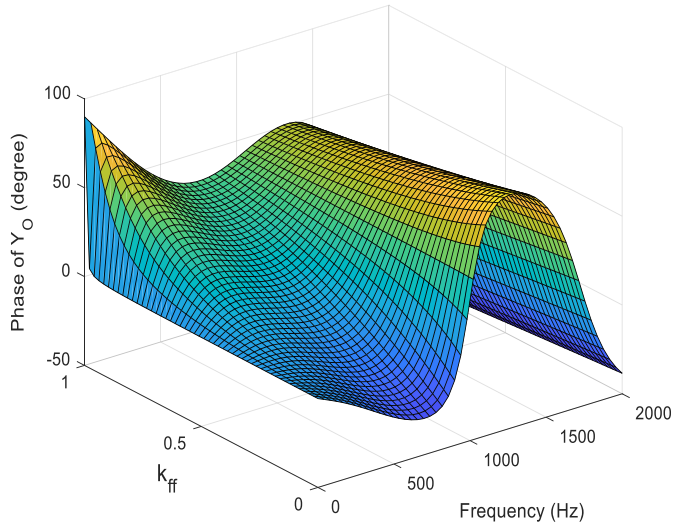

Fig. 14. Phase of inverter output admittance versus k_{ff} and frequency.

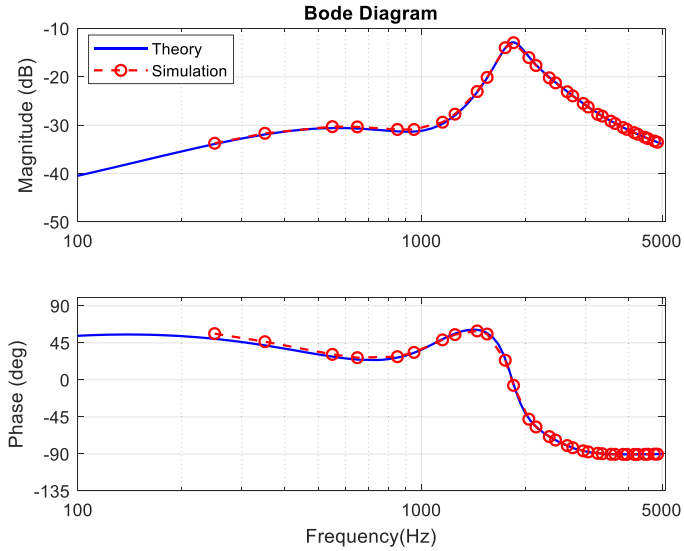

Fig. 15. Bode plot of inverter output admittance using the proposed active damping based on delay compensation and PCC voltage feedforward method.

which means the PM is improved. However, when $k_{ff} = 1$, the phase of $Y_O(s)$ is equal to about 90° in low frequencies, which is not acceptable from the power quality point of view.

According to Fig. 14, by decreasing the value of k_{ff} from 1 to 0.5, the phase of $Y_O(s)$ decreases drastically in low frequencies, while it remains acceptable in medium and high frequencies. In this paper, $k_{ff} = 0.9$ is selected, which is a tradeoff between acceptable PM for low and medium frequencies. The Bode plot of inverter output admittance [see (17)] using the proposed active damping based on delay compensation and PCC voltage feedforward method is shown in Fig. 15. Compared with Fig. 11(b), not only the non-passive region is mitigated, but also the phase of $Y_O(s)$ is reduced significantly. The peak phase value of $Y_O(s)$ is about 56°, which means PM = 34° in a pure inductive grid,

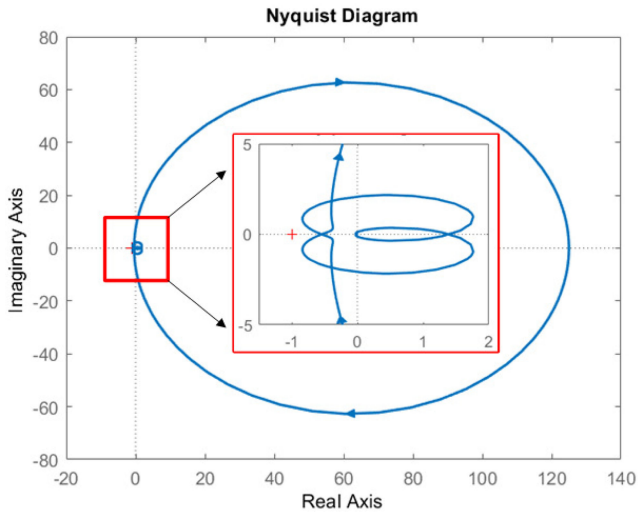

Fig. 16. Nyquist plot of the control system loop gain using the proposed methods.

which is the worst-case condition. The inverter output admittance that is measured using simulation results is also shown in Fig. 15. The measurement procedure *of* $Y_O(s)$ is similar to [38]. In this way, the voltage harmonics up to 100th harmonic component (5000 Hz) are applied at grid voltage (V_g), while the inverter reference current (i_{ref}) is set to 0. Then, the fast Fourier transform of grid injected current (I_g) is calculated and subsequently the simulation results for $Y_O(s)$ $(Y_{O\_\text{sim}}(j\omega))$ can be achieved as follows:

$$Y_{O\_\text{sim}}(j\omega) = \frac{|I_g(j\omega)|}{|V_g(j\omega)|}\exp^{[\angle I_g(j\omega)-\angle V_g(j\omega)]}. \tag{20}$$

As shown in Fig. 15, $Y_{O\_\text{sim}}(j\omega)$ well match the theoretical expression given by (17). Thanks to the proposed methods, the phase of inverter output admittance is within $[-90°, 90°]$, with a satisfying PM. This PM guarantees the stability and acceptable transient response of grid-connected inverter without worrying about the value of grid impedance and the number of parallel inverters. Hence, the inverter has plug-and-play functionality, which is the main contribution of this paper.

The Nyquist plot of the control system loop gain is shown in Fig. 16. It can be concluded from this figure that the control system is stable thanks to the proposed methods since it does not encircle the critical point $(-1, \text{j}0)$.

V. Experimental Results

In order to verify the effectiveness of the proposed delay compensation and the PCC voltage feedforward method, an experimental setup is built up in the laboratory, as shown in Fig. 17. The setup consists of three-phase *Danfoss* 2.2 kW inverters with *LCL* filters. The control algorithm is implemented in *dSPACE 1006* platform for real-time control and a *Chroma 61845* grid-simulator is used as the utility grid. The grid and inverter parameters are listed in Table I. The per-unit values are referred to the grid effective voltage Vg = 400 V and to the rated power

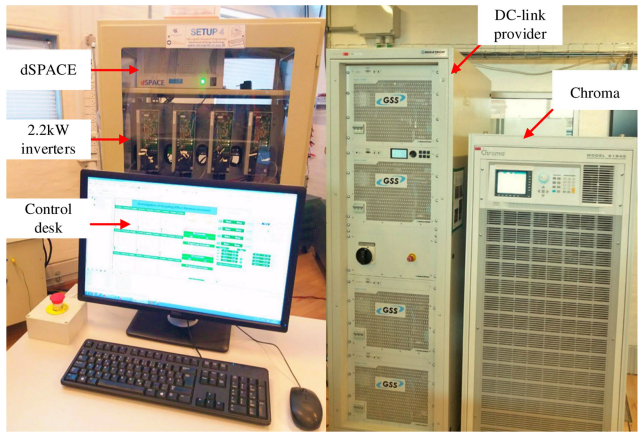

Fig. 17. Experimental setup.

TABLE II
Control Parameters

Current controller	
k_p	25
k_r	800
Active damping controller $G_{ad}(s)$	
K_{ad}	400
α	0.15
β	1
ω_α	$0.15\omega_s$
ω_β	$0.7\omega_s$
PCC voltage feedforward controller $G_{ff}(s)$	
k_{ff}	0.9
ω_{ff}	$2\pi\times2000$

2.2 kW ($Z_{\text{base}} = 72.7\ \Omega$). The control parameters are presented in Table II.

A. Effectiveness of the Proposed Delay Compensation Method

In [20], it was shown that a system without using active damping will be stable if the resonance frequency is greater than $f_s/6$. However, this feature is not attractive in practice, because the wide variation of grid impedance can shift the resonance frequency below $f_s/6$. Therefore, using the damping method is necessary for weak grid applications. However, in case of using the traditional active damping method, if the grid inductance reduces and causes $f_r > f_s/6$, the system will be unstable [19]. Hence, a delay compensation method is vital for expanding the critical frequency (f_{cr}).

According to the above-mentioned discussion and to show the effectiveness of the proposed delay compensation method for expanding the critical frequency, the following experiments are carried out. In the first step, the PCC voltage feedforward controller is deactivated $(G_{ff}(s) = 0)$ and only a proportional controller is used for active damping to show the shortcoming of the traditional active damping method. In this experiment, $K_{ad} = 15$ is selected according to [19] for stability requirements, while in the next experiments, the proposed active damping controller based on delay compensation is implemented using Table II parameters.

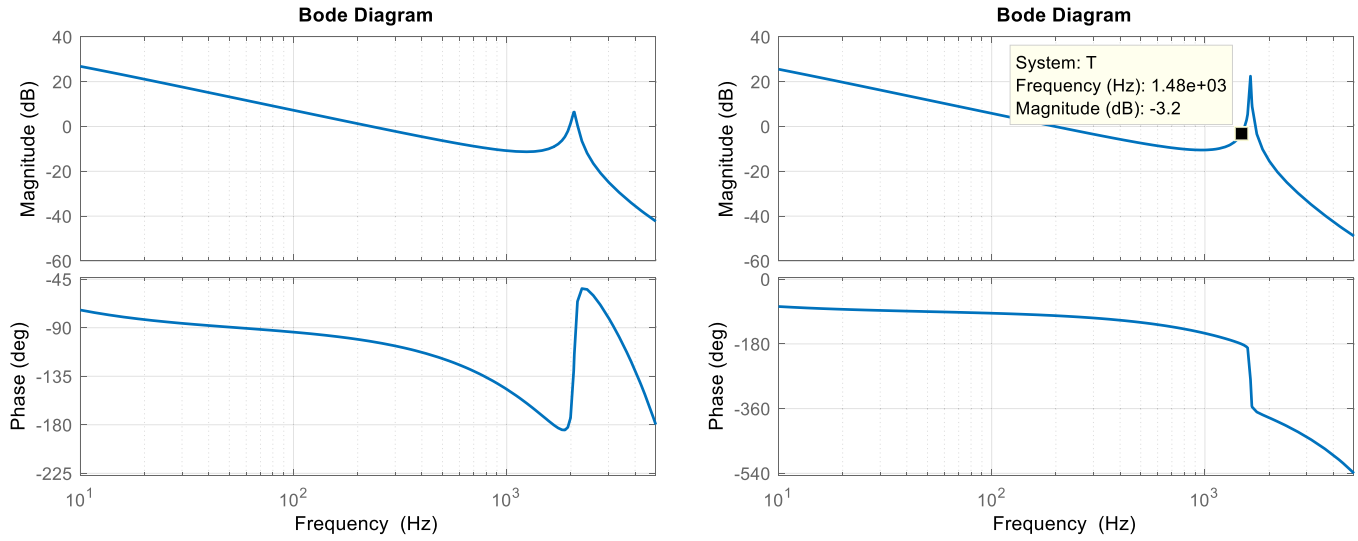

(a) (b)

Fig. 18. Bode plot of the control system loop gain using the traditional active damping. (a) $L_g = 0$. (b) $L_g = 1.8\,\text{mH}\,(0.0078\,\text{p.u.})$.

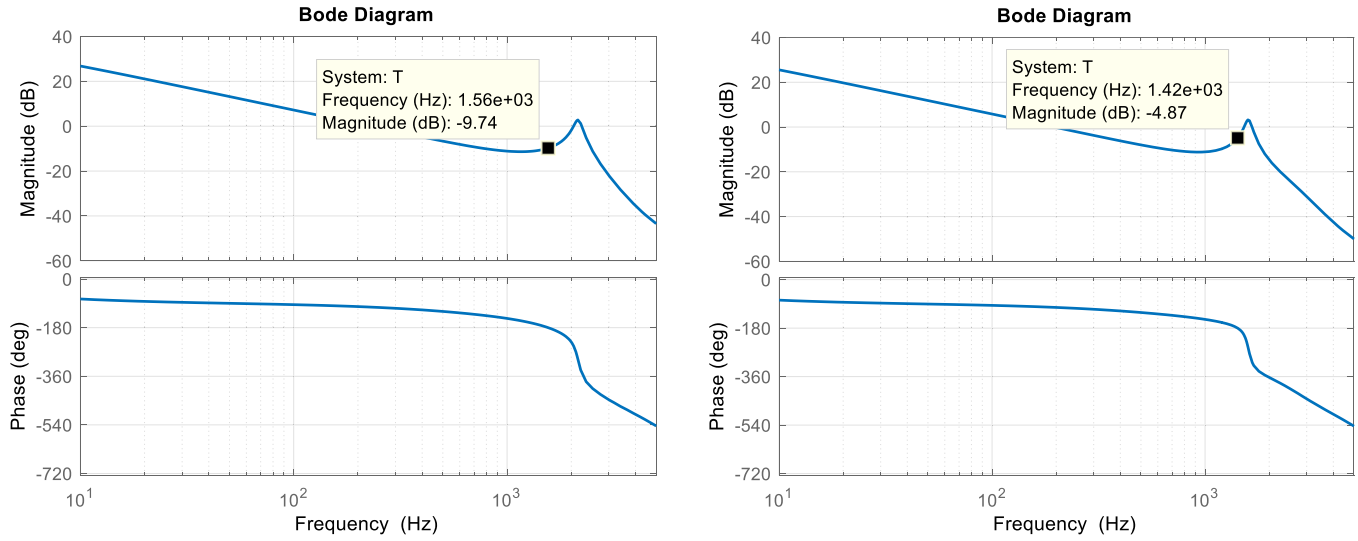

(a) (b)

Fig. 19. Bode plot of the control system loop gain using the proposed active damping. (a) $L_g = 0$. (b) $L_g = 1.8\,\text{mH}\,(0.0078\,\text{p.u.})$.

In this experiment, the grid inductance is equal to 1.8 mH (0.0078 p.u.) at first and reduces to 0 at $t = 1$ s. Some inductors are used to emulate the grid impedance between PCC and *Chroma*. To show the effect of resonance frequency variation between two regions, i.e., lower than $f_s/6$ and higher than $f_s/6$, the Bode plot of the control system loop gain, $T(s)$, for traditional and proposed active damping methods are shown in Figs. 18 and 19, respectively. In these plots, the grid-side inductor and grid inductance are lumped together $(L_2 = L_2 + L_g)$ to show the introducing RHP poles in the control system when $f_r > f_s/6$. Fig. 18(a) shows the Bode plot of loop gain when $L_g = 0$ and the traditional active damping method is used only by a proportional controller. In this condition, $f_r = 1945\,\text{Hz} > f_s/6$ and as shown, the system has non-minimum phase behavior due to RHP poles caused by the delay. In other words, since the virtual impedance is negative in frequencies higher than $f_s/6$, as described in Section II-B, the system is unstable. The Bode plot of loop gain using the traditional active damping method with $L_g = 1.8\,\text{mH}\,(0.0078\,\text{p.u.})$ is shown in Fig. 18(b). In this condition, the resonance frequency moves to 1489 Hz according to (13) and is below $f_s/6$. As shown in Fig 18(b), the system is stable because PM>0 and where the phase curve crosses $-180°$, the magnitude of loop gain is below 0 dB [19]. According to Fig. 18(b), the GM = 3.2 dB, however, such a control system is

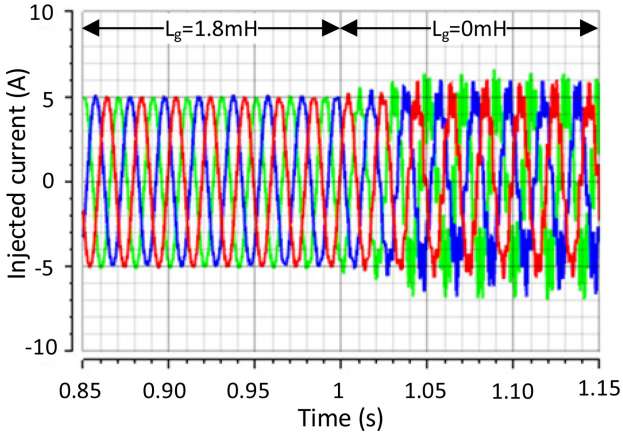

Fig. 20. Grid injected current using the traditional active damping method.

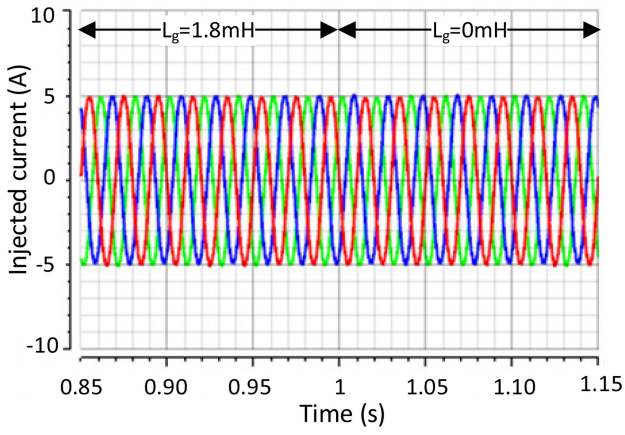

Fig. 21. Grid injected current using the proposed active damping method.

not robust, because in a weak grid, the grid inductance varies in a wide range and the system will be unstable with grid inductance reduction.

The Bode plot of loop gain using the proposed active damping based on delay compensation for $L_g = 0$ and $L_g = 1.8\,\text{mH}\,(0.0078\,\text{p.u.})$ are shown in Fig. 19(a) and (b), respectively. As shown in these plots, thanks to the biquad filter and expanding the critical frequency, the control system is stable regardless of resonance frequency variation. The GMs are 9.74 dB and 4.87 dB, respectively. According to these figures, the proposed active damping controller is capable of resonance damping either $f_r < f_s/6$ or $f_r > f_s/6$.

To show the validity of the above-mentioned analytical results, an experiment is carried out using traditional and proposed active damping methods. The inverter reference current (i_{ref}) is set to 5 A. The grid injected current is shown in Fig. 20, while the traditional active damping method is used. As shown in this figure, the system is stable for $L_g = 1.8\,\text{mH}\,(0.0078\,\text{p.u.})$, however, when the grid inductance reduces to zero, the resonance frequency $(f_r = 1945\,\text{Hz})$ becomes higher than $f_s/6$ and the system goes toward instability due to RHP poles caused by the delay. Fig. 20 validates the theoretical analysis and proofs that the traditional active damping method is not robust in weak grids.

In the next experiment, the proposed active damping controller (G_{ad}) based on delay compensation is used and the experimental result is shown in Fig. 21. As shown in this figure, thanks to the proposed delay compensation method, the inverter is stable in both conditions, since the critical frequency is expanded up to Nyquist frequency according to Fig. 10. The experimental results verify the theoretical analysis and show the superiority of the proposed active damping method with respect to the traditional one.

B. Passivity-Based Stability Enhancement Using PCC Voltage Feedforward Method

As shown in Figs. 11(b) and 12, despite using the proposed active damping based on delay compensation, it would remain a narrow region in the vicinity of resonance frequency at which the phase of inverter output admittance is beyond $[-90°, 90°]$

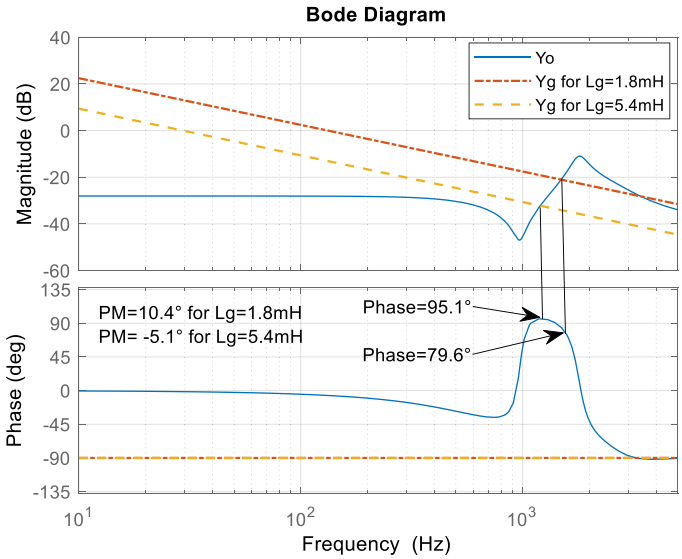

Fig. 22. Bode plots of Y_O and Y_g without using the proposed PCC voltage feedforward method.

or PM is insufficient. The former will cause instability and the latter will cause poor power quality when the grid admittance and inverter output admittance magnitudes intersect in such region. The Bode plot of the inverter output admittance as well as grid admittance for $L_g = 1.8\,\text{mH}\,(0.0078\,\text{p.u.})$ and $L_g = 5.4\,\text{mH}\,(0.0233\,\text{p.u.})$ are shown in Fig. 22, without using the proposed PCC voltage feedforward method. As shown in this figure, when $L_g = 1.8\,\text{mH}\,(0.0078\,\text{p.u.})$, the inverter output admittance intersects with grid admittance in the passive region with PM $= 10.4°$, therefore, the control system is stable. However, when the grid inductance increases to 5.4 mH (0.0233 p.u.), $Y_O(s)$ and $Y_g(s)$ intersect in the non-passive region where PM $= -5.1°$, which shows that the system is unstable.

This problem is solved using the proposed PCC voltage feedforward method. The Bode plot of the inverter output admittance using the proposed PCC voltage feedforward shown in Fig. 23 shows that the system is stable despite wide variation of grid

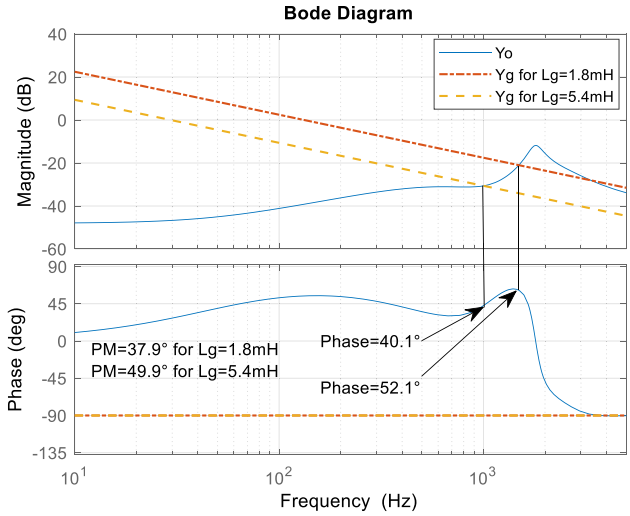

Fig. 23. Bode plots of Y_O and Y_g using the proposed PCC voltage feedforward method.

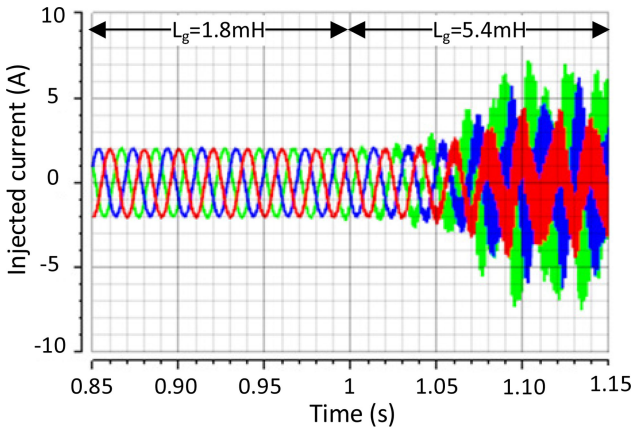

Fig. 24. Grid injected current without using the proposed PCC voltage feedforward when the grid inductance changes from 1.8 mH (0.0078 p.u.) to 5.4 mH (0.0233 p.u.).

inductance. To verify the above-mentioned analysis, new experiments are carried out with and without using the proposed PCC voltage feedforward method. The grid injected current without using the PCC feedforward method is shown in Fig. 24, when the grid inductance changes from 1.8 mH (0.0078 p.u.) to 5.4 mH (0.0233 p.u.) at $t = 1$ s. Due to prevent the operation of protective relays in unstable condition, the magnitude of i_{ref} is set to 2 A in this experiment. As shown in this figure, the grid injected current is stable when $L_g = 1.8\,\text{mH}\,(0.0078\,\text{p.u.})$, however, it goes toward instability with increasing of grid inductance. The experimental result using the proposed PCC voltage feedforward method is shown in Fig. 25. As expected, the inverter is stable regardless of grid inductance variation thanks to the proposed method.

C. Stability Investigation Against the Number of Parallel Inverters

In a microgrid with n similar paralleled inverters and Z_g as grid impedance, the grid equivalent impedance that is seen by each inverter is n times of Z_g $(n \times Z_g)$ [28]. Therefore, the number of inverters can endanger the overall system stability.

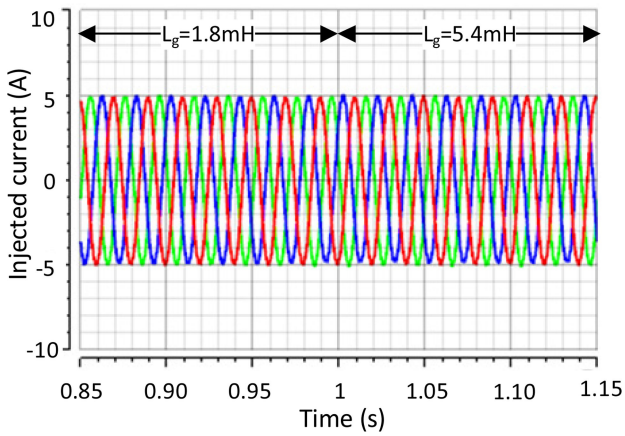

Fig. 25. Grid injected current using the proposed PCC voltage feedforward when the grid inductance changes from 1.8 mH (0.0078 p.u.) to 5.4 mH (0.0233 p.u.).

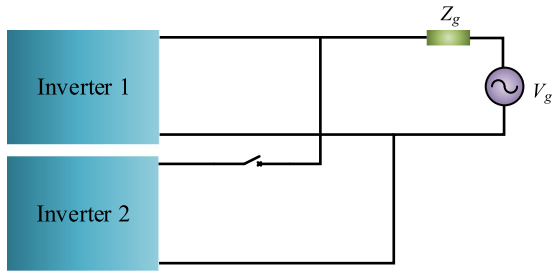

Fig. 26. Topology of two paralleled grid-connected inverters.

To show the superiority of the proposed methods in multi-paralleled systems, parallel connection of two grid-connected inverters is considered as Fig. 26 where $L_g = 1.8\,\text{mH}\,(0.0078\,\text{p.u.})$. The Bode plots of inverter output admittance with and without using the proposed PCC voltage feedforward method are shown in Fig. 27. According to [28], the equivalent grid inductance is $L_{\text{eq\_}g} = 2L_g = 3.6\,\text{mH}\,(0.0156\,\text{p.u.})$, and Bode plot of its admittance $(Y_{\text{eq\_}g})$ is shown in Fig. 27 as well. As shown in this figure, without using the proposed PCC voltage feedforward method, the inverter output admittance intersects with $Y_{\text{eq\_}g}$ within the non-passive frequency range, which will cause instability.

However, in case of using the proposed PCC voltage feedforward method, the intersection point is always in the passive region. Fig. 28 shows the experimental result without using the PCC voltage feedforward method. In this case, inverter 1 injects its current to the grid and at $t = 1$ s, inverter 2 connects to the grid. As shown in this figure, before connection of inverter 2, inverter 1 is stable and injects a clean current to the grid. However, after connection of inverter 2, whole of the system becomes unstable since equivalent grid inductance is increased.

This experiment is repeated using the proposed PCC voltage feedforward method and its result is shown in Fig. 29. As shown in this figure, the system remains stable after connection of inverter 2, thanks to the proposed method that keeps the phase

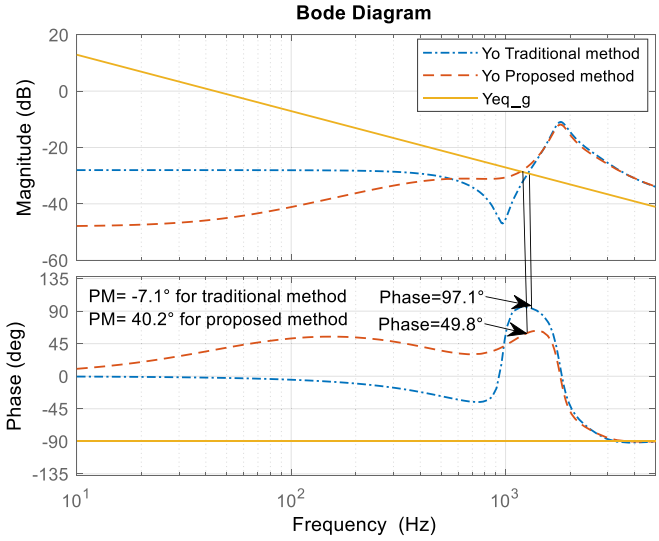

Fig. 27. Bode plots of the inverter output admittance Y_O with and without using the PCC voltage feedforward method as well as equivalent grid admittance $Y_{\mathrm{eq\_}g}$.

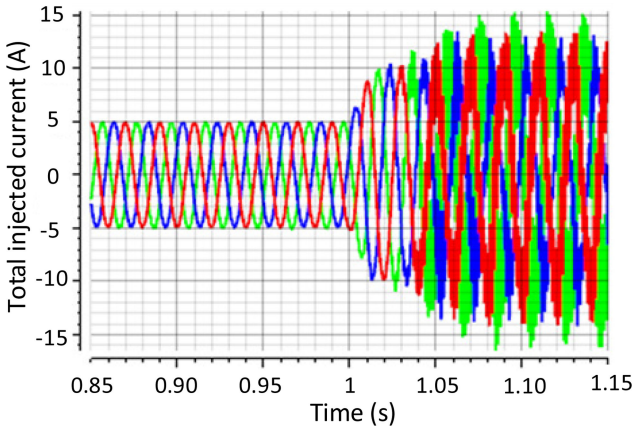

Fig. 28. Grid injected current of two inverters without using the proposed PCC voltage feedforward method.

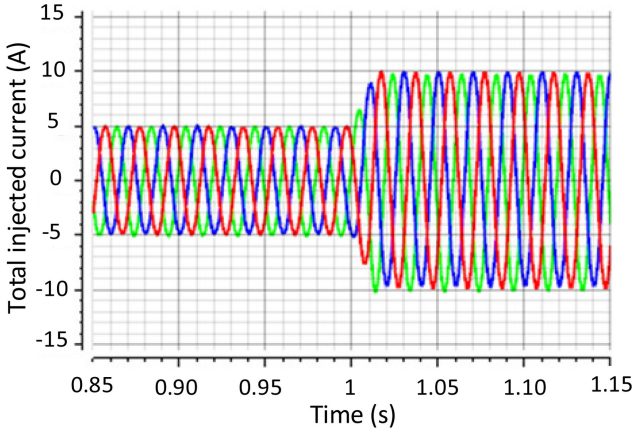

Fig. 29. Grid injected current of two inverters using the proposed PCC voltage feedforward method.

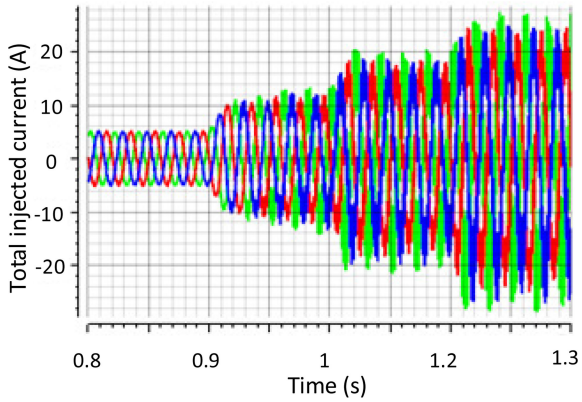

Fig. 30. Grid injected current of four inverters without using the proposed PCC voltage feedforward method.

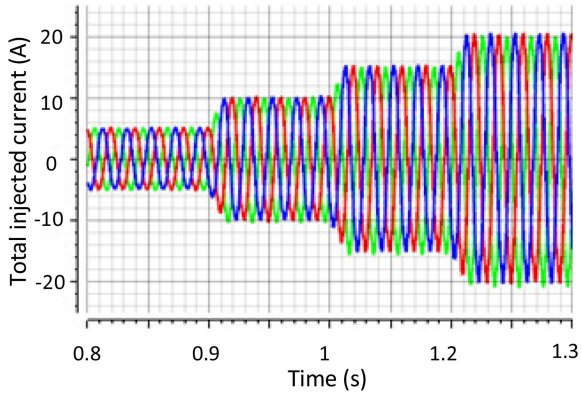

Fig. 31. Grid injected current of four inverters using the proposed PCC voltage feedforward method.

of the inverter output admittance within the passive area with a sufficient PM. The experimental results validate the analytical results derived from Fig. 27.

For the sake of generality, parallel connection of four inverters is examined in the following. In this scenario, the inverters are connected to the grid one by one. Fig. 30 shows the total grid injected current without using the PCC voltage feedforward method. As shown in this figure, after connection of second inverter, the total grid injected current becomes unstable and it remains so, by connection of other inverters. The experimental result in case of using the proposed PCC voltage feedforward method is shown in Fig. 31. As expected, the total grid injected current is stable regardless of number of inverters thanks to the proposed method.

The proposed method can be used for control system design of multi-paralleled grid-connected inverters without considering the coupling effect of inverters in control system design step. In this way, the tedious computations of multi-input multi-output control systems analysis in [28] and [29] are not needed.

D. Transient Response and Steady-State Current Quality Comparison

In order to show the superiority of the proposed PCC voltage feedforward method in transient and steady-state conditions, a

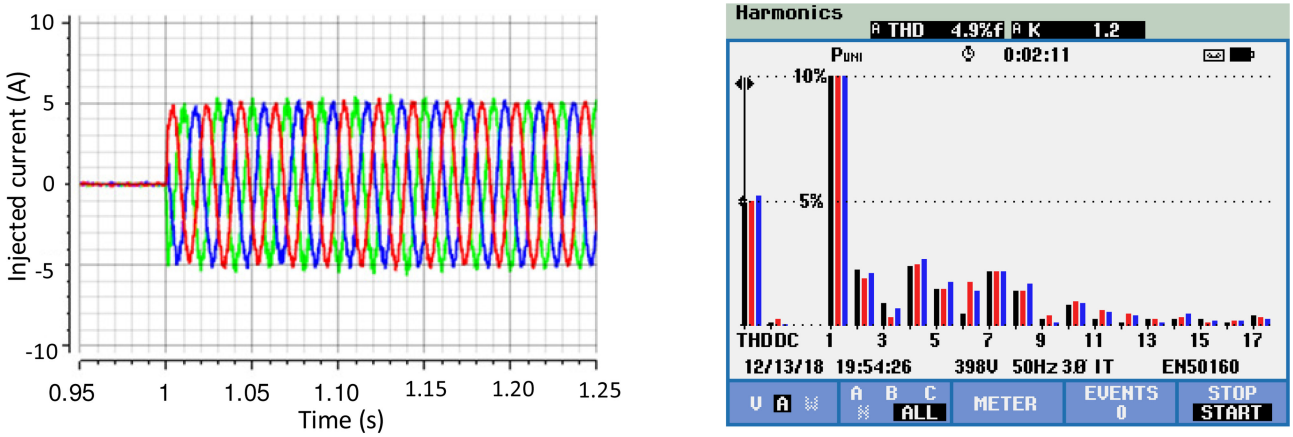

(a) (b)

Fig. 32. (a) Step change of reference current without using the proposed PCC voltage feedforward method. (b) Harmonic spectrum of grid injected current in steady state.

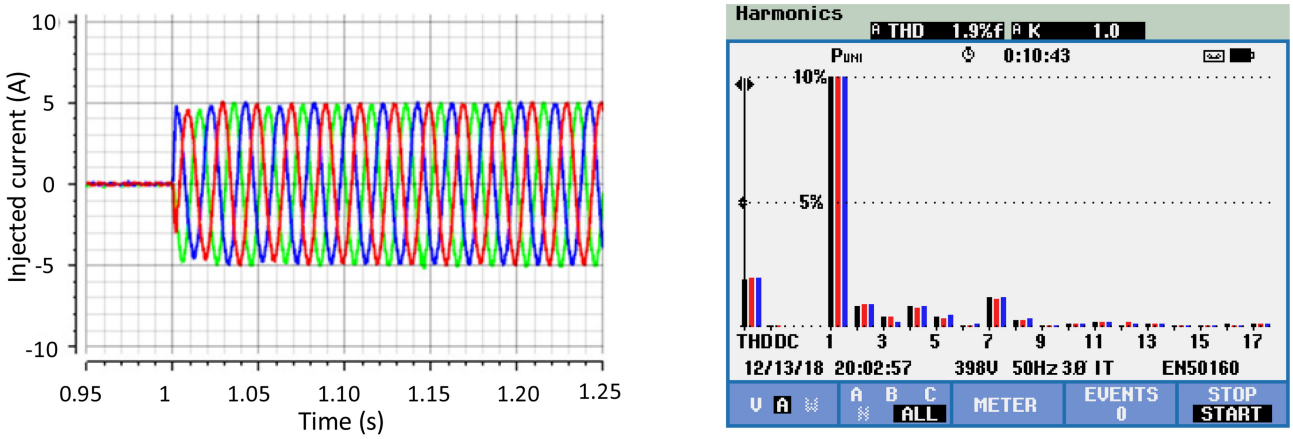

(a) (b)

Fig. 33. (a) Step change of reference current using the proposed PCC voltage feedforward method. (b) Harmonic spectrum of grid injected current in steady state.

step change from zero to nominal value in reference injected current is carried out. In this experiment, the grid inductance is $L_g = 1.8\,\text{mH}\,(0.0078\,\text{p.u.})$ and the system is stable, without using the proposed PCC voltage feedforward method. According to Fig. 22, the PM is relatively low (PM $= 10.4°$) and the inverter might have relatively poor power quality. The transient response and quality of the grid injected current are investigated in this section. The grid injected current without using the PCC voltage feedforward method is shown in Fig. 32(a). Also, the harmonic spectrum of the grid-injected current in steady-state condition is shown in Fig. 32(b).

The experimental results in case of using the proposed PCC voltage feedforward method are shown in Fig. 33. Results comparison in Figs. 32(a) and 33(a) shows that the harmonic content of the grid injected current is decreased due to PM increment in case of using the proposed method. Also, the total harmonic distortion (THD) value of the grid injected current is decreased from 4.9% to 1.9%, which shows that the proposed method can improve the quality of grid injected current.

The experimental results verify that the proposed control system provides plug-and-play functionality for the inverter and so it can be connected to the grid without worrying about grid impedance variation and the number of parallel inverters.

VI. Conclusion

This paper presents a control system for stable and acceptable operation of *LCL*-filtered grid-connected inverters in weak grids with wide variation of grid impedance. At first, it was shown that in the traditional active damping method, the time delay of digitally controlled systems causes an unintentionally negative virtual resistance when the resonance frequency is higher than one-sixth of the sampling frequency $(f_s/6)$. To overcome this problem, a delay compensation method based on a biquad

filter is proposed, which is capable of expanding the effective damping region up to the Nyquist frequency $(f_s/2)$, which is a great improvement. Therefore, the *LCL* filter can be designed without worrying about *LCL* filter resonance frequency. Then, the passivity-based stability is enhanced to remain the phase of inverter output admittance within $[-90°, 90°]$, with a satisfying PM. To do this, a PCC voltage feedforward method is proposed that is capable of mitigating the non-passive region and guaranteeing the acceptable operation of grid-connected inverters. The control system robustness is validated in case of grid impedance wide variation and connection of new parallel inverters using comprehensive analysis and experimental results. Therefore, the proposed control system provides plug-and-play functionality for the inverter.

REFERENCES

[1] IEEE Standard for Interconnecting Distributed Resources With Electric Power Systems, IEEE Standard 1547, 2003.

[2] Electromagnetic Compatibility (EMC)—Part 3-2: Limits—Limits for Harmonic Current Emissions (Equipment Input Current $\leq$16 A Per Phase), IEC 61000-3-2, ed. 5, 2018.

[3] S. Jayalath and M. Hanif, "Generalized *LCL*-filter design algorithm for grid-connected voltage-source inverter," *IEEE Trans. Ind. Electron.*, vol. 64, no. 3, pp. 1905–1915, Mar. 2017.

[4] X. Ruan, X. Wang, D. Pan, D. Yang, W. I. Li, and C. Bao, "Resonance damping methods of *LCL* filter," in *Control Techniques for LCL-Type Grid-Connected Inverters*. Beijing, China: Springer, 2018, ch. 4, pp. 79–93.

[5] R. Peña-Alzola, M. Liserre, F. Blaabjerg, R. Sebastián, J. Dannehl, and F. W. Fuchs, "Analysis of the passive damping losses in *LCL*-filter-based grid converters," *IEEE Trans. Power Electron.*, vol. 28, no. 6, pp. 2642–2646, Jun. 2013.

[6] X. Wang, X. Ruan, S. Liu, and C. K. Tse, "Full feedforward of grid voltage for grid inverter with *LCL* filter to suppress current distortion due to grid voltage harmonics," *IEEE Trans. Power Electron.*, vol. 25, no. 12, pp. 3119–3127, Dec. 2010.

[7] X. Wang, F. Blaabjerg, and P. C. Loh, "Virtual *RC* damping of *LCL*-filtered voltage source converters with extended selective harmonic compensation," *IEEE Trans. Power Electron.*, vol. 30, no. 9, pp. 4726–4737, Sep. 2015.

[8] X. Wang, F. Blaabjerg, and P. C. Loh, "Grid-current-feedback active damping for *LCL* resonance in grid-connected voltage-source converters," *IEEE Trans. Power Electron.*, vol. 31, no. 1, pp. 213–223, Jan. 2016.

[9] D. Pan, X. Ruan, C. Bao, W. Li, and X. Wang, "Capacitor-current-feedback active damping with reduced computation delay for improving robustness of *LCL*-type grid connected inverter," *IEEE Trans. Power Electron.*, vol. 29, no. 7, pp. 3414–3427, Jul. 2014.

[10] S. Y. Park, C. L. Chen, J. S. Lai, and S. R. Moon, "Admittance compensation in current loop control for a grid-tie *LCL* fuel cell inverter," *IEEE Trans. Power Electron.*, vol. 23, no. 4, pp. 1716–1723, Jul. 2008.

[11] Y. Jia, J. Zhao, and X. Fu, "Direct grid current control of *LCL*-filtered grid-connected inverter mitigating grid voltage disturbance," *IEEE Trans. Power Electron.*, vol. 29, no. 3, pp. 1532–1541, Mar. 2014.

[12] J. Xu, S. Xie, and T. Tang, "Active damping-based control for grid-connected *LCL*-filtered inverter with injected grid current feedback only," *IEEE Trans. Ind. Electron.*, vol. 61, no. 9, pp. 4746–4758, Sep. 2014.

[13] M. H. Mahlooji, H. R. Mohammadi, and M. Rahimi, "A review on modeling and control of grid-connected photovoltaic inverters with *LCL* filter," *Renew. Sustain. Energy Rev.*, vol. 81, pp. 563–578, Jan. 2018.

[14] J. Liu, L. Zhou, B. Li, C. Zheng, and B. Xie, "Modeling and analysis of a digitally controlled grid-connected large-scale centralized PV system," *IEEE Trans. Power Electron.*, vol. 33, no. 5, pp. 4000–4014, May 2018.

[15] X. Zhang, P. Chen, C. Yu, F. Li, H. T. Do, and R. Cao, "Study of a current control strategy based on multisampling for high-power grid-connected inverters with an *LCL* filter," *IEEE Trans. Power Electron.*, vol. 32, no. 7, pp. 5023–5034, Jul. 2017.

[16] A. Aapro, T. Messo, T. Roinila, and T. Suntio, "Effect of active damping on output impedance of three-phase grid-connected converter," *IEEE Trans. Ind. Electron.*, vol. 64, no. 9, pp. 7532–7541, Sep. 2017.

[17] Y. Lyu, H. Lin, and Y. Cui, "Stability analysis of digitally controlled *LCL*-type grid-connected inverter considering the delay effect," *IET Power Electron.*, vol. 8, no. 9, pp. 1651–1660, Aug. 2015.

[18] J. Yin, S. Duan, and B. Liu, "Stability analysis of grid-connected inverter with *LCL* filter adopting a digital single-loop controller with inherent damping characteristic," *IEEE Trans. Ind. Inf.*, vol. 9, no. 2, pp. 1104–1112, May 2013.

[19] X. Ruan, X. Wang, D. Pan, D. Yang, W. I. Li, and C. Bao, "Resonance damping methods of *LCL* filter," in *Control Techniques for LCL-Type Grid-Connected Inverters*. Beijing, China: Springer, 2018, ch. 8, pp. 165–196.

[20] S. G. Parker, B. P. McGrath, and D. G. Holmes, "Regions of active damping control for *LCL* filters," *IEEE Trans. Ind. Appl.*, vol. 50, no. 1, pp. 424–432, Jan./Feb. 2014.

[21] D. Pan, X. Ruan, C.Bao, W. Li, and X. Wang, "Capacitor-current-feedback active damping with reduced computation delay for improving robustness of *LCL*-type grid-connected inverter," *IEEE Trans. Power Electron.*, vol. 29, no. 7, pp. 3414–3427, Jul. 2014.

[22] Z. Xin, X. Wang, P. C. Loh, and F. Blaabjerg, "Grid-current-feedback control for *LCL*-filtered grid converters with enhanced stability," *IEEE Trans. Power Electron.*, vol. 32, no. 4, pp. 3216–3228, Apr. 2017.

[23] X. Li, X. W. Y. Geng, X. Yuan, C. Xia, and X. Zhang, "Wide damping region for *LCL*-type grid-connected inverter with an improved capacitor current-feedback method," *IEEE Trans. Power Electron.*, vol. 30, no. 9, pp. 5247–5259, Sep. 2015.

[24] Q. Qian, S. Xie, L. Huang, J. Xu, Z. Zhang, and B. Zhang, "Harmonic suppression and stability enhancement for parallel multiple grid-connected inverters based on passive inverter output impedance," *IEEE Trans. Ind. Electron.*, vol. 64, no. 9, pp. 7587–7598, Sep. 2017.

[25] V. Miskovic, V. Blasko, T. Jahns, A. Smith, and C. Romenesko, "Observer based active damping of *LCL* resonance in grid connected voltage source converters" in *Proc. IEEE Energy Convers. Congr. Expo.*, 2013, pp. 4850–4856.

[26] L. Zhou *et al.*, "Robust two degrees-of-freedom single-current control strategy for *LCL*-type grid-connected DG system under grid-frequency fluctuation and grid-impedance variation," *IET Power Electron.*, vol. 9, no. 14, pp. 2682–2691, Nov. 2016.

[27] X. Chen, Y. Zhang, S. Wang, J. Chen, and C. Gong, "Impedance-phased dynamic control method for grid-connected inverters in a weak grid," *IEEE Trans. Power Electron.*, vol. 32, no. 1, pp. 274–283, Jan. 2017.

[28] J. L. Agorreta, M. Borrega, J. López, and L. Marroyo, "Modeling and control of *N*-paralleled grid-connected inverters with *LCL* filter coupled due to grid impedance in PV plants," *IEEE Trans. Power Electron.*, vol. 26, no. 3, pp. 770–785, Mar. 2011.

[29] A. Akhavan, H. R. Mohammadi, and J. M. Guerrero, "Modeling and design of a multivariable control system for multi-paralleled grid-connected inverters with *LCL* filter," *Int. J. Elect. Power Energy Syst.*, vol. 94, pp. 354–362, Jan. 2018.

[30] C. Yoon, H. Bai, R. N. Beres, X. Wang, C. L. Bak and F. Blaabjerg, "Harmonic stability assessment for multiparalleled, grid-connected inverters," *IEEE Trans. Power Electron.*, vol. 7, no. 4, pp. 1388–1397, Oct. 2016.

[31] J. Sun, "Impedance-based stability criterion for grid-connected inverters," *IEEE Trans. Power Electron.*, vol. 26, no. 11, pp. 3075–3078, Nov. 2011.

[32] L. Jia, X. Ruan, W. Zhao, Z. Lin, and X. Wang, "An adaptive active damper for improving the stability of grid-connected inverters under weak grid," *IEEE Trans. Power Electron.*, vol. 33, no. 11, pp. 9561–9574, Nov. 2018.

[33] J. Xu, S. Xie, and T. Tang, "Improved control strategy with grid-voltage feedforward for *LCL*-filter-based inverter connected to weak grid," *IET Power Electron.*, vol. 7, no. 10, pp. 2660–2671, Oct. 2014.

[34] L. Harnefors, X. Wang, A. Yepes, and F. Blaabjerg, "Passivity-based stability assessment of grid-connected VSCs—An overview," *IEEE J. Emerg. Sel. Topics Power Electron.*, vol. 4, no. 1, pp. 116–125, Mar. 2016.

[35] H. Bai, X. Wang, P. C. Loh, and F. Blaabjerg, "Passivity enhancement of grid-tied converters by series *LC*-filtered active damper," *IEEE Trans. Ind. Electron.*, vol. 64, no. 1, pp. 369–379, Jan. 2017.

[36] Y. He, H. S. Chung, C. Lai, X. Zhang, and W. Wu, "Active cancelation of equivalent grid impedance for improving stability and injected power quality of grid-connected inverter under variable grid condition," *IEEE Trans. Power Electron.*, vol. 33, no. 11, pp. 9387–9398, Nov. 2018.

[37] X. Wang, F. Blaabjerg, and P. C. Loh, "Passivity-based stability analysis and damping injection for multiparalleled VSCs with *LCL* filters," *IEEE Trans. Power Electron*, vol. 32, no. 11, pp. 8922–8935, Nov. 2017.

[38] E. Rodriguez-Diaz, F. D. Freijedo, J. M. Guerrero, J. Marrero-Sosa, and D. Dujic, "Input-admittance passivity compliance for grid-connected converters with an *LCL* Filter," *IEEE Trans. Ind. Electron.*, vol. 66, no. 2, pp. 1089–1097, Feb. 2019.

[39] Z. Zhang, W. Wu, and F. Blaabjerg, "Principle and robust impedance-based design of grid-tied inverter with *LLCL*-filter under wide variation of grid-reactance," *IEEE Trans. Power Electron.*, vol. 34, no. 5, pp. 4362–4374, May 2019.
[40] L. Harnefors, A. G. Yepes, A. Vidal, and J. Doval-Gandoy, "Passivity-based controller design of grid-connected VSCs for prevention of electrical resonance instability," *IEEE Trans. Ind. Electron.*, vol. 62, no. 2, pp. 702–710, Feb. 2015.
[41] T. Messo, J. Jokipii, A. Mäkinen, and T. Suntio, "Modeling the grid synchronization induced negative-resistor-like behavior in the output impedance of a three-phase photovoltaic inverter," in *Proc. IEEE 4th Int. Symp. Power Electron. Distrib. Gener. Syst.*, 2013, pp. 1–8.
[42] B. Wen, D. Boroyevich, P. Mattavelli, Z. Shen, and R. Burgos, "Influence of phase-locked loop on input admittance of three-phase voltage-source converters," in *Proc. 28th Annu. IEEE Appl. Power Electron. Conf. Expo.*, 2013, pp. 897–904.
[43] A. Kuperman, "Proportional-resonant current controllers design based on desired transient performance," *IEEE Trans. Power Electron.*, vol. 30, no. 10, pp. 5341–5345, Oct. 2015.
[44] A. G. Yepes, F. D. Freijedo, J. Doval-Gandoy, Ó. López, J. Malvar, and P. Fernandez-Comesaña, "Effects of discretization methods on the performance of resonant controllers," *IEEE Trans. Power Electron.*, vol. 25, no. 7, pp. 1692–1712, Jul. 2010.
[45] D. Pan, X. Ruan, and X. Wang, "Direct realization of digital differentiators in discrete domain for active damping of *LCL*-type grid-connected inverter," *IEEE Trans. Power Electron.*, vol. 33, no. 10, pp. 8461–8473, Oct. 2018.

Ali Akhavan was born in Kashan, Iran, in 1990. He received the B.S., M.S., and Ph.D. degrees in electrical engineering from the University of Kashan, Kashan, Iran, in 2012, 2014, and 2019, respectively.

He was a Ph.D. Guest with the Department of Energy Technology, Aalborg University, Aalborg, Denmark, from July 2018 to February 2019. His research interests include power electronics, modeling and control of grid-connected converters, stability analysis, and different microgrid aspects.

Hamid Reza Mohammadi (M'17) was born in Qom, Iran, in 1971. He received the B.S. degree in electrical engineering from Sharif University of Technology, Tehran, Iran, in 1993, the M.S. degree in electrical engineering from the University of Tabriz, Tabriz, Iran, in 1995, and the Ph.D. degree in electrical engineering from Tarbiat Modares University, Tehran, in 2008.

Since 2008, he has been an Assistant Professor with the Department of Electrical Engineering, University of Kashan, Kashan, Iran. His research interests include power electronics, power quality, active filters, and different microgrid aspects including modeling and control of power converters, power quality, and energy management.

Juan C. Vasquez (M'12–SM'14) received the B.S. degree in electronics engineering from the Autonomous University of Manizales, Manizales, Colombia, and the Ph.D. degree in automatic control, robotics, and computer vision from the Technical University of Catalonia, Barcelona, Spain, in 2004 and 2009, respectively.

In 2011, he was an Assistant Professor and from 2014, he is currently an Associate Professor with the Department of Energy Technology, Aalborg University, Aalborg, Denmark, where he is the Vice Programme Leader of the Microgrids Research Program. His current research interests include operation, advanced hierarchical and cooperative control, optimization and energy management applied to distributed generation in ac/dc microgrids, maritime microgrids, advanced metering infrastructures, and the integration of Internet of Things into the SmartGrid.

Josep M. Guerrero (S'01–M'04–SM'08–F'15) received the B.S. degree in telecommunications engineering, the M.S. degree in electronics engineering, and the Ph.D. degree in power electronics from the Technical University of Catalonia, Barcelona, Spain, in 1997, 2000, and 2003, respectively.

Since 2011, he has been a Full Professor with the Department of Energy Technology, Aalborg University, Aalborg, Denmark, where he is responsible for the Microgrid Research Program. In 2012, he was a Guest Professor with the Chinese Academy of Science and the Nanjing University of Aeronautics and Astronautics, and in 2014, he was the Chair Professor with Shandong University. His research interests include different microgrid aspects, including power electronics, distributed energy-storage systems, hierarchical and cooperative control, energy management systems, smart metering and the Internet of Things for ac/dc microgrid clusters, and islanded minigrids.

Prof. Guerrero was awarded by Thomson Reuters as an ISI Highly Cited Researcher.